

# Measuring Disturbance Response of a Fully-Actuated UAV using Surging Flow Wind Tunnel Experiments

J. Chen\*, N.J. Kay and K.A. Stol

Department of Mechanical and Mechatronics Engineering, University of Auckland, New Zealand

## ABSTRACT

This paper presents a novel experimental setup in a wind tunnel that is capable of measuring the frequency response of an over-actuated Unmanned Aerial Vehicle (UAV). The setup generates wind surges with a sinusoidal time response, allowing for free-flight testing of the UAV at various frequencies. Importantly, the surging flow method employed in this study offers a predictable and repeatable experiment compared to other wind tunnel tests that utilised turbulence grids. The closed-loop frequency response of the UAV to wind disturbances is plotted, revealing peaks in the gain response that are not present in simulated results. These unexpected peaks identify that system dynamics that are not modelled in the simulation are present in the physical system.

These findings demonstrate the effectiveness of the experimental setup and provide valuable insights into the UAV's response to disturbances.

## 1 INTRODUCTION

Unmanned aerial vehicles (UAVs) have experienced a large growth in popularity in the past few decades in both commercial and academic sectors. With the miniaturisation of sensors and embedded computers, small multirotor UAVs in particular are becoming a widely used instrument in a variety of fields such as surveillance, mapping, agriculture and delivery due to features such as their agility and relatively moderate production costs [1, 2, 3].

Conventional UAV designs have all rotors applying force in a parallel direction to counteract gravity and thus under-actuated dynamics due to the coupling between the horizontal translational and rotational dynamics. Fully-actuated UAVs are a type of UAV that have an equal number of control inputs to the number of degrees of freedom (DoF), and each DoF is decoupled and can thus be controlled by an independent control input. This class of UAVs is able to apply forces in a plane perpendicular to the rotor axis making them more suitable than conventional designs for certain tasks, examples being aerial physical interaction and wind gust rejection [4, 5].

Over-actuated UAVs are another type of UAV that share similar characteristics to fully-actuated UAVs with added redundant control inputs, allowing for greater fault tolerance and robustness.

The optimal rotor configuration for fully-actuated UAV designs is often application-dependent, where different configurations are more suitable for certain design goals, such as better dynamic maneuverability, minimum energy consumption, greater force bandwidth or wrench generation [3]. Different control algorithms have also been developed throughout literature to utilise the advantages of these configurations [6, 7]. Examples of small fully-actuated and over-actuated multirotor UAVs have been developed by several researchers, demonstrating their potential for high levels of maneuverability [8, 9, 10, 11].

With the increased popularity of UAVs, there is an increased need for accurate flight performance while resisting external disturbances due to factors such as wind, aerodynamic ground effects or when performing aerial manipulation [12]. Accurate modeling of the dynamics of these UAVs is thus crucial for improving their performance through better design and control. Many research groups have made use of various analytical and empirical methods to derive UAV aerodynamics [13, 14, 15], which can then be used to develop suitable simulation models for controller design and testing. Modelling has been shown to be a useful tool for understanding the behavior of multirotor UAVs but may not capture all of its complexities accurately due to unmodelled dynamics. Experimental methods are then used to validate and refine these UAV models.

Free-flight testing is a widely used approach in UAV literature to assess the vehicle's dynamics and performance in real-world environments [16, 17, 18]. This method involves flying the UAV under various conditions, and comparing the recorded data with simulation results to evaluate the aircraft's performance. Outdoor testing provides the most realistic representation of real-world conditions but introduces uncertainties and limited control over external factors. Indoor testing offers controlled conditions but are limited by space restrictions.

Wind tunnel testing, on the other hand, provides controlled experimental conditions for UAV flight. Although the wind tunnel environment does not fully replicate the real-world wind conditions and turbulence experienced during outdoors flight, its predictable nature offers distinct advantages for precise and repeatable assessment of the stability

\*Email address(es): jche825@aucklanduni.ac.nz

and control of the vehicle. Additionally, the use of motion capture systems in the wind tunnel setting enables highly accurate data collection, which may be challenging to achieve or cost-prohibitive in outdoor environments. The effectiveness of wind tunnel testing has been demonstrated in examples such as [19, 20], in which testing was performed using either constant wind, or turbulent wind which contains a broad spectrum of irregular wind speeds.

In past literature, it was noted that some fully-actuated drones have an advantage over under-actuated drones in terms of actuator bandwidth or rise time [9, 21]. The irregularity of turbulent wind was found to be unsuitable for properly evaluating the effects of this advantage. To investigate this advantage, equipment was built by Buchanan [22] to generate predictable sinusoidal wind 'surges' which are described in [23] and hereon referred to as 'surging flow'. To the author's knowledge, UAV free-flight testing has yet to be performed under the conditions described. This paper therefore extends work done in [20] by investigating the frequency response of a fully-actuated UAV in free-flight using surging flow conditions generated by a wind tunnel.

The paper is organised as follows. In Section 2, the fully-actuated UAV and testing environment are introduced. The experimental process and results are then discussed in Section 3, and finally the conclusions drawn and future work are summarised in Section 4.

## 2 SETUP DESCRIPTION

### 2.1 UAV Airframe and Controller

This section introduces the UAV investigated in this paper, known as the canted-rotor planar octorotor (CRPO) UAV, which was previously designed in research conducted at the university [20]. As the CRPO has 8 control inputs for 6 DoF of motion, it is technically an over-actuated UAV, however it is treated as a fully-actuated UAV as this characteristic is not explored in this paper.

Two different reference frames are used in this paper. One is about the *body* of the aircraft, denoted as  $B[x, y, z]$  about the forward, right and down directions of the aircraft respectively. Additionally, euler angles for roll  $\psi$ , pitch  $\theta$  and yaw  $\phi$  of the aircraft are positive clockwise about these three respective body axes. The *world* coordinate frame then describes the environment the aircraft is in  $W[x, y, z]$  where the  $W_{xy}$ -plane is parallel to the ground,  $W_z$  is positive upwards normal to the ground, and centred on the ground in the flight zone described later in Section 2.2.

The CRPO is similar to a conventional planar octorotor UAV, except the rotors of the CRPO have been canted such that adjacent propellers are tilted along the  $B_x$ - and  $B_y$ -axes at a fixed angle  $\zeta$  in opposing pairs, as shown in Figure 1. This allows for decoupling of position and attitude control, where increasing thrust from certain rotors while decreasing thrust from others generates a net thrust along its  $B_{xy}$ -plane without generating moments or affecting the net force normal

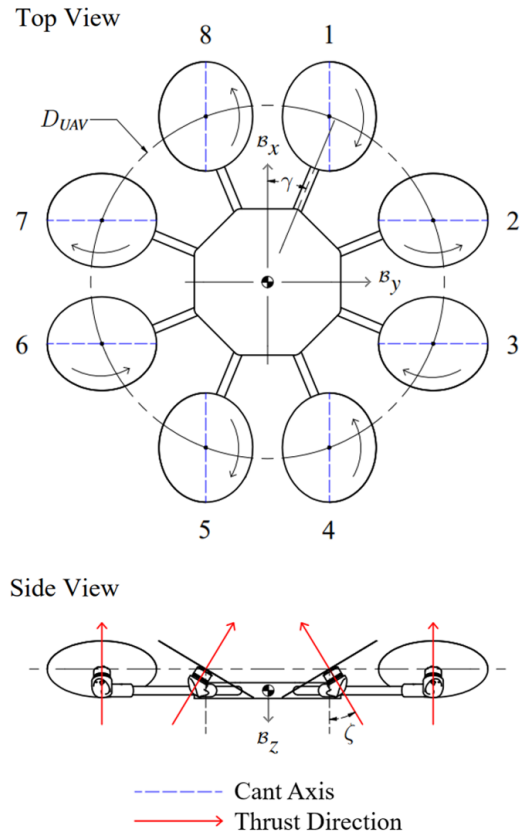


Figure 1: Diagram of the canted-rotor planar octorotor UAV

to this plane in the  $B_z$  direction.

The CRPO is able to produce thrust in the world  $W_x$ - and  $W_y$ -axes using two different methods: directly via body thrust as described above, or in a manner similar to an under-actuated UAV by first tilting the aircraft so the  $B_z$ -axis thrust has components in the  $W_x$ - or  $W_y$ -axes. These two actuation methods will hereon be described as *vectored thrust* and *attitude-based thrust* respectively. Experiments showed that the bandwidth of vectored thrust compared to attitude-based thrust was 8Hz and 1.7Hz respectively, suggesting vectored thrust was better suited for counteracting high frequency disturbances. However, attitude-based thrust was determined to be capable of producing a higher magnitude of force in the  $W_{xy}$ -plane.

The CRPO UAV model was primarily constructed using carbon fibre plates and tubes. It is controlled by a Holybro Pixhawk 4 flight controller running PX4 Autopilot. The CRPO is equipped with a radio module for manual operation via a radio controller, as well as a WiFi module for communication with a ground control station (GCS) laptop using the MAVLink protocol. The aircraft has a rotor-to-rotor diameter  $D_{UAV}$  of 0.5m and a flight mass of 1.72kg. An image of the aircraft is provided in Figure 2.

The CRPO can be operated with two different position



Figure 2: Photo of the canted-rotor planar octorotor UAV

controllers: a baseline PX4 controller based on PID, which does not utilize vectored thrust, or an  $H-\infty$  controller designed by Bannwarth [20]. The  $H-\infty$  controller is a linear multivariable control system, which was optimised to mitigate disturbances based on a linearised model of the aircraft constructed at a station-keeping operating point in a 5.6m/s headwind. The controller takes advantage of the strengths of the CRPO's separate actuation methods by individually penalising inputs and outputs based on frequency. This approach is thus able to leverage the higher frequency bandwidth enabled by vectored thrust as well as the greater magnitude of thrust provided through attitude-based thrust.

The design features of the CRPO and a system of equations representing its dynamics and aerodynamics are described in greater detail by Chen and Bannwarth et al. in [21, 24]. Bannwarth also describes how the system of equations were then used to construct a simulation model of the plant and controller in MATLAB Simulink. The structure of this simulation model is shown in Figure 3 and it is used later in Section 3 to generate simulated results for comparison with the experimental data.

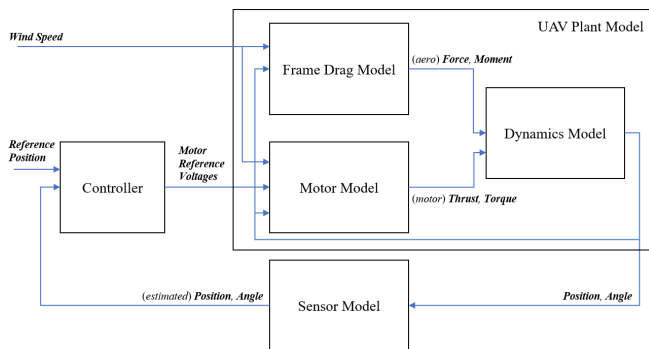


Figure 3: CRPO Simulation Model

2.2 Surging Flow System

The flight environment used in this experiment to generate surging flow is the University of Auckland's Boundary Layer Wind Tunnel (BLWT). Detailed descriptions for the wind tunnel and modifications made in the flight zone to

enable free flight testing and surging flow can be found in [15, 20, 22, 25]. This section will briefly summarise its key features in relation to the free-flight tests that were conducted in this paper.

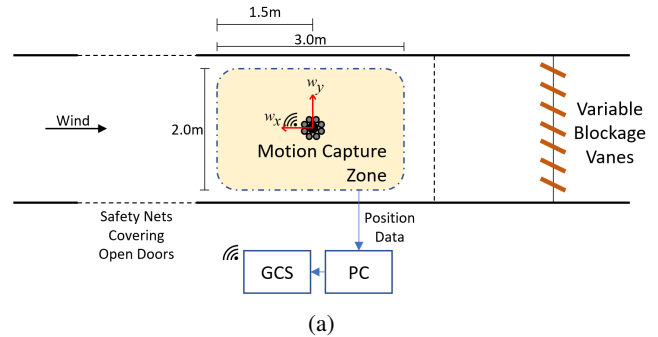


Figure 4: a) Diagram of BLWT flight zone and b) photo of BLWT flight zone taken from upstream

The BLWT is a closed-loop wind tunnel with a 20m test section that is 3.6m in width and 2.5m in height. Within this test section there is a much smaller motion capture zone suitable for free-flight experiments that is 2.0m in width and 3.0m in length. Figure 4a shows the layout of the flight environment for this experiment within the test section of the wind tunnel. The wind tunnel is able to generate wind speeds within the tunnel of up to  $20m.s^{-1}$ . This has been restricted to a maximum of  $10m.s^{-1}$  for safety reasons in the experiments conducted due to the flow blockage caused by the variable blockage vanes. Wind speed in the tunnel is tracked in two locations both upstream and downstream of the test area by pitot tubes.

The variable blockage vanes are a set of seven motorised vanes, shown as the vertical wooden slats downstream of the tunnel in Figure 4b. The angle of these vanes can be adjusted from an open angle of  $0^\circ$  shown in the Figure to a closed angle of  $90^\circ$  to increase blockage within the tunnel and thus de-

http://www.imavs.org/

crease wind speed in the testing zone separately from the primary wind tunnel fan. To reduce pressure loading on the wind tunnel fans, the tunnel side doors must be left open when the vanes are operating and thus nets have been placed across the doors and behind the flight zone for safety.

The vanes are able to repeatedly generate discrete one-dimensional (1-D) gusts of wind in the  $^Wx$ -axis with minimal turbulence. This can be controlled to generate a 'surging flow', or a set of gusts with speeds that resemble a 1-D sinusoidal signal in the time domain, and thus a single frequency component. The frequency of these wind gusts is determined by the frequency the vanes are operating and the gust amplitude is related to the turning angle of the vane, e.g. a surging flow may be generated using sweeps between only  $0^\circ$  to  $30^\circ$ . Characterisation of the wind generated by this system has been conducted by Kay et al. in past research and can be found in [23].

The motion capture zone shown in Figure 4 provides accurate position and attitude data with sub-millimetre position accuracy. Motion capture is performed by twelve Opti-Track Flex 3 cameras, shown embedded in the roof in Figure 4b, which track circular reflective markers on the object of interest. Several of these markers can be seen attached to the body of the CRPO in Figure 2.

The localisation of position data is achieved by processing the camera feeds on a PC, which transmits the data to a ground control station (GCS) laptop. The GCS laptop runs the MAVROS package and establishes a connection to the UAV through a Wi-Fi module. By utilising this Wi-Fi connection, the position data is transmitted to the UAV flight controller using MAVLink messages. On the UAV, the received position data is filtered with on-board sensor data, thus minimising errors associated with sensor inaccuracies.

### 3 SURGING FLOW EXPERIMENTS

During these station-keeping experiments, power was supplied to the CRPO by a power supply via tether, allowing for greater flight endurance. The flight mass mentioned at the end of Section 2.1 includes the mass of this tether and the power supply Voltage is set to 12.6V to simulate a 3S Lithium-Polymer battery.

To maintain consistency between experiments, it is desirable that the mean wind speed and amplitude are constant for all surging flow frequencies. However, when the variable blockage vanes described in Section 2.2 are in operation the mean wind speed decreases significantly from the open-vane wind speed; this drop changes with both surging flow frequency and vane angle. Similarly, the amplitude of wind gusts is also affected by both maximum vane turn angle and frequency. For example, to achieve wind speeds with a mean, amplitude and frequency of  $5.6\text{ms}^{-1}$ ,  $0.56\text{ms}^{-1}$  and  $1.0\text{s}^{-1}$  (Hz) respectively, an open vane wind speed of  $8.3\text{ms}^{-1}$  was needed and vanes were swept from  $0^\circ$  to  $67^\circ$ . As such, appropriate open-vane wind speeds and vane turn angles must



Figure 5: CRPO station-keeping in the BLWT under surging flow. Wind sock visually indicates wind direction.

be selected before conducting free-flight experiments to generate a consistent set of winds for use in said experiments.

The  $H_\infty$  controller described at the end of Section 2.1 is linearised about a mean wind speed of  $5.6\text{ms}^{-1}$ , which was the target mean wind speed for free-flight experiments using a turbulence grid conducted by Bannwarth [20]. As such, this wind speed  $U_{mean} = 5.6\text{ms}^{-1}$  was again chosen to be the mean wind speed for the surging flow experiments conducted in this paper. To remain within the linearised region, wind speed amplitude  $U_{amp}$  was then set to a small value; this was chosen as 10% of the mean wind speed or  $0.56\text{ms}^{-1}$ . Experiments were then conducted across a range of frequencies  $f = \{0.05, 0.1, 0.2, 0.3, 0.4, 0.5, 0.6, 0.7, 0.8, 1.0\}$ . Experiments were also repeated using both a baseline PX4 controller based off of PID and the  $H_\infty$  controller. To ensure the desired mean and amplitude wind speeds at each frequency, interpolation was applied to wind profiling data collected by Kay et al. [23] and confirmed experimentally using a Cobra probe 3-axis wind sensor placed at the station-keeping position of the CRPO in the experiment, described later in Section 3.1. During this stage, wind profile logs were also collected, providing data on wind speeds within the flight zone in relation to the variable vane turn angle.

#### 3.1 Experiment Procedure

During the experiment the CRPO is set to *offboard*-mode, which is an autonomous mode where the UAV receives a constant stream of position setpoints for the desired hover position,  $^Wx_{ref} = [0 \ 0 \ 1.25]^T$  m. This corresponds to a location 1.25m above the centre of the motion capture area, aligned with the centre of the wind tunnel and is the position the UAV will attempt to hold during the experiment. The  $H_\infty$  controller is turned on here if appropriate for the experiment.

Once the wind tunnel is activated, the wind speed is gradually increased to the desired open-vane wind speed. Sufficient time is allowed for the wind speed to reach a steady state within the tunnel. Subsequently, the variable-blockage vanes

are activated, and their operation is sustained for a duration of 40 seconds to 2 minutes, depending on the test frequency. This ensures that the surging flow within the tunnel achieves a steady state for a meaningful period. A photo taken during one test flight can be seen in Figure 5.

During the experiment flight logs were recorded, capturing aircraft position, attitude, and control allocation data. These logs were subsequently processed to extract flight data aligned with the variable vane turn angle. A sample from one experiment can be seen in Figure 6, after synchronising time between the aircraft log and profiled wind data. Curve fitting tools have been used to approximate the shape of the responses and most importantly the amplitudes of each response, which are then used to generate the plots discussed in Section 3.2.

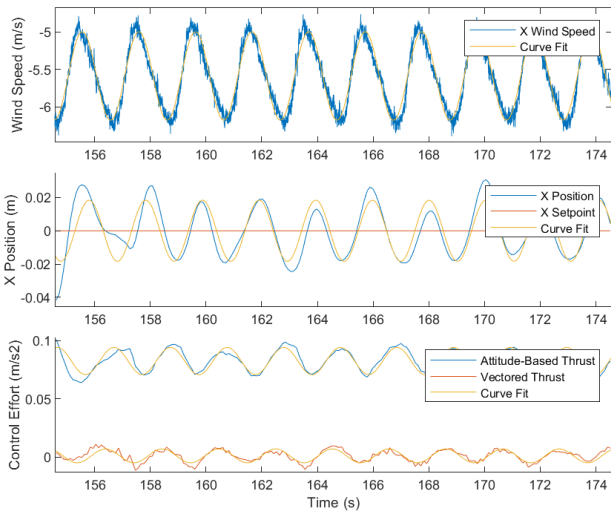


Figure 6: Combined logs from CRPO station-keeping in the BLWT using the H-∞ controller under 0.5Hz surging flow. From the top, graphs represent estimated wind speed, UAV position and UAV control effort in the  $w_x$ -axis

### 3.2 Experiment Results

Results for each experiment were recollected by using the wind profile logs collected as inputs to the simulation model described in Figure 3. The closed-loop frequency response to wind disturbance from both simulation and experimental results for both baseline and H-∞ controllers is then shown in Figure 7. In this graph, "Position Gain" represents the difference in decibels between the output position amplitude when fitted to a sinusoidal curve and the input wind speed amplitude when fitted to a sinusoidal curve at each frequency. Although not all signals exhibited perfect sinusoidal behavior, especially at lower frequencies with minimal position deviation, the analysis revealed that sinusoidal curve fits yielded satisfactory results. Specifically, the simulated results consistently achieved an R-squared value above 0.8, indicating a

strong fit to the sinusoidal curve. Similarly, the experimental results exhibited an R-squared value above 0.7, indicating an acceptable level of accuracy for the curve fits. Despite some deviations from ideal sinusoidal patterns, the overall quality of the fits suggests their suitability for the analysis and interpretation of the data.

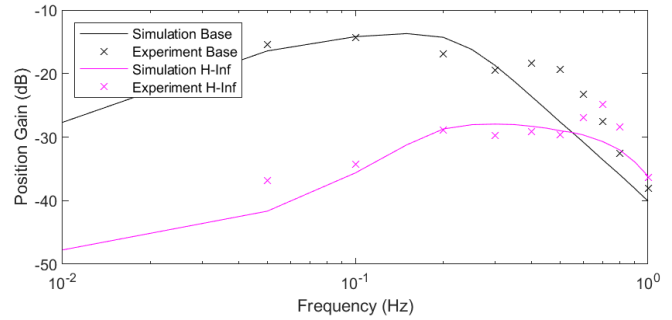


Figure 7: Closed-loop frequency response of position error gain due to wind disturbance

The simulated results appear to represent the performance of the real system in free-flight experiments fairly accurately except for around the 0.4Hz and the 0.7Hz region for baseline and H-∞ controllers respectively where there appears to be an additional peak in the results from free-flight experiments. It is likely that these peaks were caused by unmodelled or inaccurately modelled system dynamics, such as the influence of the power tether on the UAV's mass moment of inertia  $I$  in the experiment. Furthermore, the variations in damping effects induced by the different controllers may contribute to the disparate frequencies at which these peaks occur.

Additionally, it was previously difficult to experimentally confirm whether the frequency-based control allocation of the H-∞ controller described in Section 2.1 was effective at mitigating position gain. By analysing control allocation at each frequency, Figure 8 demonstrates that in relation to position error amplitude, control effort of the vectored thrust appears to increase more significantly than attitude-based thrust with surging flow frequency.

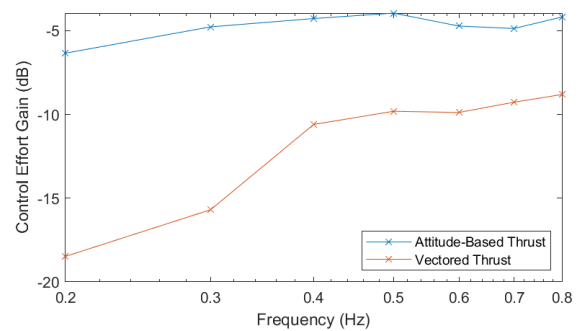


Figure 8: Closed-loop frequency response of control effort gain due to position error of the H-∞ controller

http://www.imavs.org/

#### 4 CONCLUSION

In this study, we have introduced a novel experimental setup in a wind tunnel to measure the disturbance response of a fully-actuated UAV. By generating wind surges with a sinusoidal shape, we conducted free-flight tests across a range of winds with a single frequency component, enabling the analysis of the UAV's closed-loop frequency response to wind disturbances.

We observed an unexpected peak in the closed-loop frequency response of the position error of the CRPO found through the surging flow wind tunnel experiments that wasn't present in simulated experiments. This difference identifies the effect that the unmodelled dynamics in the physical system, such as the effects of the power supply tether or frame vibrations, has on results from experiments using the CRPO. Additionally, this apparatus was used to investigate the effect of frequency-weighted control of the two separate actuation methods for horizontal thrust of the CRPO when using the  $H_\infty$  controller, and the results aligned well with expectations for the performance of its frequency weighting.

These findings highlight the usefulness of this experimental setup for identifying unmodelled dynamics and investigating control strategies of over-actuated UAVs.

##### 4.1 Future Work

Further investigation could be performed on several areas identified by this work. Firstly, the sources of the unexpected peaks in the frequency response should be examined, and the unmodelled dynamics should be identified to further refine the simulation model and controller. Surging flow experiments could then be used to validate the accuracy of these changes.

Furthermore, the frequency response analysis of the UAV's dynamics offers valuable insights for refinement of the UAV's design and control system. For the case of the  $H_\infty$  controller, by examining performance across different frequencies, a more effective frequency weighting may be applied to reduce gain at specific frequencies and thus improve overall performance. Surging flow experiments could then be used to investigate the effectiveness of these changes at specific surging flow frequencies.

#### ACKNOWLEDGMENTS

The research reported in this article was conducted as part of "Enabling unmanned aerial vehicles (UAVs) to use tools in complex dynamic environments UOCX2104", which is funded by the New Zealand Ministry of Business, Innovation and Employment.

#### REFERENCES

- [1] F. Nex, C. Armenakis, M. Cramer, D.A. Cucci, M. Gerke, E. Honkavaara, A. Kukko, C. Persello, and J. Skaloud. Uav in the advent of the twenties: Where we stand and what is next. *ISPRS Journal of Photogrammetry and Remote Sensing*, 184:215–242, 2022.
- [2] Bas Vergouw, Huub Nagel, Geert Bondt, and Bart Custers. *Drone Technology: Types, Payloads, Applications, Frequency Spectrum Issues and Future Developments*, pages 21–45. T.M.C. Asser Press, The Hague, 2016.
- [3] S. Suzuki. Recent researches on innovative drone technologies in robotics field. *Advanced Robotics*, 32(19):1008–1022, 2018.
- [4] Yuichi Tadokoro, Tatsuya Ibuki, and Mitsuji Sampei. Classification and structural evaluation of fully-actuated hexrotor uavs. In *2018 Annual American Control Conference (ACC)*, pages 1945–1950. IEEE, 2018.
- [5] Ramy Rashad, Jelmer Goerres, Ronald Aarts, Johan B. C. Engelen, and Stefano Stramigioli. Fully actuated multirotor uavs: A literature review. *IEEE Robotics & Automation Magazine*, 27(3):97–107, 2020.
- [6] Jinho Kim, S. Andrew Gadsden, and Stephen A. Wilkerson. A comprehensive survey of control strategies for autonomous quadrotors. *Canadian Journal of Electrical and Computer Engineering*, 43(1):3–16, 2020.
- [7] Sherif I. Abdelmaksoud, Musa Mailah, and Ayman M. Abdallah. Control strategies and novel techniques for autonomous rotorcraft unmanned aerial vehicles: A review. *IEEE Access*, 8:195142–195169, 2020.
- [8] Z. Jeremy Chen, Karl A. Stol, and Peter J. Richards. Preliminary design of multirotor uavs with tilted-rotors for improved disturbance rejection capability. *Aerospace Science and Technology*, 92:635–643, 2019.
- [9] Guangying Jiang and Richard Voyles. A nonparallel hexrotor uav with faster response to disturbances for precision position keeping. In *2014 IEEE International Symposium on Safety, Security, and Rescue Robotics (2014)*, pages 1–5, 2014.
- [10] Sijia Wang, Lei Ma, Binbin Li, and Kai Zhang. Architecture design and flight control of a novel octopus shaped multirotor vehicle. *IEEE Robotics and Automation Letters*, 7(1):311–317, 2022.
- [11] Florentin von Frankenberg and Scott Nokleby. Disturbance rejection in multi-rotor unmanned aerial vehicles using a novel rotor geometry. In *Proc. 4th Int. Conf. Control Dynamic Systems and Robotics*, 2017.
- [12] Pedro Sanchez-Cuevas, Guillermo Heredia, and Anibal Ollero. *Multirotor Aerodynamic Effects in Aerial Manipulation*, pages 67–82. Springer International Publishing, Cham, 2019.

- [13] Nedim Osmić, Muhamed Kurić, and Ivan Petrović. Detailed octorotor modeling and pd control. In *2016 IEEE International Conference on Systems, Man, and Cybernetics (SMC)*, pages 002182–002189, 2016.
- [14] Praveen Abbaraju, Xin Ma, Guangying Jiang, Mo Rastgaar, and Richard M. Voyles. Aerodynamic modeling of fully-actuated multirotor uavs with nonparallel actuators. In *2021 IEEE/RSJ International Conference on Intelligent Robots and Systems (IROS)*, pages 9639–9645, 2021.
- [15] Jérémie X. J. Bannwarth, Z. Jeremy Chen, K. A. Stol, B. A. MacDonald, and P. J. Richards. Development of a wind tunnel experimental setup for testing multirotor unmanned aerial vehicles in turbulent conditions. In *2018 IEEE/ASME International Conference on Advanced Intelligent Mechatronics (AIM)*, pages 724–729, 2018.
- [16] Nicolas Michel, Peng Wei, Zhaodan Kong, Anish Kumar Sinha, and Xinfan Lin. Modeling and validation of electric multirotor unmanned aerial vehicle system energy dynamics. *eTransportation*, 12:100173, 2022.
- [17] Christina Ivler, Robert Niemiec, Farhan Gandhi, and Frank C Sanders. Multirotor electric aerial vehicle model validation with flight data: Physics-based and system identification models. In *Vertical Flight Society 75th Annual Forum, Philadelphia, PA, USA*, 2019.
- [18] He Zhu, Hong Nie, Limao Zhang, Xiaohui Wei, and Ming Zhang. Design and assessment of octocopter drones with improved aerodynamic efficiency and performance. *Aerospace Science and Technology*, 106:106206, 2020.
- [19] Fu Junquan, Gong Zheng, Shi Zhiwei, Zhang Tongren, and Zhu Jiachen. Transition controllability research on tri-tilt rotor unmanned aerial vehicle in wind tunnel free flight tests. In *2017 9th International Conference on Modelling, Identification and Control (ICMIC)*, pages 527–532, 2017.
- [20] Jérémie X. J. Bannwarth. *Aerodynamic Modelling and Wind Disturbance Rejection of Multirotor Unmanned Aerial Vehicles*. PhD thesis, University of Auckland, Auckland, New Zealand, 2021.
- [21] Z. Jeremy Chen, Jérémie X. J. Bannwarth, Karl A. Stol, and Peter J. Richards. Analysis of a multirotor uav with tilted-rotors for the purposes of disturbance rejection. In *2018 International Conference on Unmanned Aircraft Systems (ICUAS)*, pages 864–873, 2018.
- [22] Rory D. Buchanan. Aerodynamic modelling and rejection of wind disturbances for multirotor unmanned aerial vehicles. Master’s thesis, University of Auckland, Auckland, New Zealand, 2020.
- [23] Nicholas J. Kay, Rory D. Buchanan, Peter J. Richards, and Karl A. Stol. Generating sinusoidal flow surges in a large closed-loop wind tunnel. In *16th International Conference on Wind Engineering*, to appear.
- [24] Jérémie X. J. Bannwarth, Z. Jeremy Chen, Karl A. Stol, Bruce A. MacDonald, and Peter J. Richards. Aerodynamic force modeling of multirotor unmanned aerial vehicles. *AIAA Journal*, 57(3):1250–1259, 2019.
- [25] Richard G. J. Flay and Yin Fai Li. New zealand country report 2021. *Construction*, 2:65–77, December 2022.